Elsevier Editorial System(tm) for Atmospheric Research
Manuscript Draft

Manuscript Number:

Title: Assimilating surface data into a mesoscale model ensemble: Cold pool analyses from spring 2007

Article Type: 4ECSS Special Issue

Section/Category:

Keywords: Data assimilation; surface observations; mesoscale analysis; cold pools

Corresponding Author: Dr. David Stensrud,

Corresponding Author's Institution:

First Author: David J Stensrud

Order of Authors: David J Stensrud; David Stensrud; Nusrat Yussouf; David C Dowell; Michael C Coniglio

Abstract: Hourly mesoscale analyses are created through an ensemble Kalman filter assimilation of 2-m potential temperature, 2-m dewpoint temperature, and 10-m wind observations into the Weather Research and Forecast (WRF-ARW) model using the Data Assimilation Research Testbed (DART) framework. Hourly analyses are created from 1300 UTC to 0600 UTC each day from 15 March through 30 June 2007. Two cases in which a distinct isolated mesoscale convective system is seen in observations are selected for further examination. Results indicate that the ensemble mean surface analyses reproduce the surface mesoscale features associated with cold pools underneath these precipitating systems in agreement with available observations. However, the ensemble Kalman filter also is able to produce vertical motion fields and vertical structures within and above the boundary layer that are consistent with these observed surface features. In particular, a rear inflow jet is produced at roughly 1 km above ground level behind the main convective line along with an "onion" sounding along the back edge of the trailing stratiform precipitation region near a surface mesolow. Both of these structures are known to be associated with MCSs and the ability of the ensemble Kalman filter assimilation to produce these important mesoscale features is encouraging.

Assimilating surface data into a mesoscale model ensemble: Cold pool analyses from spring 2007

David J. Stensrud[a], Nusrat Yussouf[a,b], David C. Dowell[c], and Michael C. Coniglio[a,b]

[a]*NOAA/National Severe Storms Laboratory, National Weather Center, 120 David L. Boren Blvd., Norman, OK 73072, USA*
[b]*Cooperative Institute for Mesoscale Meteorological Studies, National Weather Center, 120 David L. Boren Blvd., Norman, OK, 73072, USA*
[c]*National Center for Atmospheric Research, P. O. Box 3000, Boulder, CO, 80307, USA*

Submitted to
2007 European Conference on Severe Storms Special Issue
Atmospheric Research
27 November 2007

Corresponding author: Dr. David J. Stensrud
NOAA/National Severe Storms Laboratory, Rm. 4368
National Weather Center
120 David L. Boren Blvd.
Norman, OK 73072 USA
E-mail: David.Stensrud@noaa.gov
Phone: +1-405-325-6170
Fax: +1-405-325-2316

Abstract

Hourly mesoscale analyses are created through an ensemble Kalman filter assimilation of 2-m potential temperature, 2-m dewpoint temperature, and 10-m wind observations into the Weather Research and Forecast (WRF-ARW) model using the Data Assimilation Research Testbed (DART) framework. Hourly analyses are created from 1300 UTC to 0600 UTC each day from 15 March through 30 June 2007. Two cases in which a distinct isolated mesoscale convective system is seen in observations are selected for further examination. Results indicate that the ensemble mean surface analyses reproduce the surface mesoscale features associated with cold pools underneath these precipitating systems in agreement with available observations. However, the ensemble Kalman filter also is able to produce vertical motion fields and vertical structures within and above the boundary layer that are consistent with these observed surface features. In particular, a rear inflow jet is produced at roughly 1 km above ground level behind the main convective line along with an "onion" sounding along the back edge of the trailing stratiform precipitation region near a surface mesolow. Both of these structures are known to be associated with MCSs and the ability of the ensemble Kalman filter assimilation to produce these important mesoscale features is encouraging.

Keywords: Data assimilation; surface observations; mesoscale analysis; cold pools

1. Introduction

Surface observations provide a wealth of information on mesoscale features such as mesohighs, mesolows, drylines, frontal boundaries, sea breezes, and heat islands (Fujita 1963; Schaefer 1974; Atkinson 1981; Johnson et al. 1989). As the densest in situ operational data set available in both time and space, surface observations are commonly used to assess the evolving weather situation through the creation of frequent sub-synoptic-scale analyses (Johns and Doswell 1992). Surface analyses help forecasters identify important mesoscale features that influence local or regional weather conditions, often with an emphasis upon features that can lead to the development of convection. However, even surface observations may fail to fully sample various mesoscale features, owing to the roughly 100 km average surface station separation. Thankfully, states and private companies are deploying surface observing sites to monitor road conditions and provide local support for a wide variety of activities, leading to an ever-increasing number of surface observations (Stensrud et al. 2006). Yet the value of surface observations for short-range mesoscale numerical weather prediction still remains uncertain, perhaps due to the methods by which these observations are assimilated into models.

It is well known that the initial conditions of operational forecast models typically fail to depict mesoscale structures that are important to the development of deep convection and heavy rainfall (Olson 1985; Funk 1991; Stensrud and Fritsch 1994; Stensrud et al. 1999; Gallus and Segal 2001). One of the most important mesoscale structures is the surface cold pool, a coherent low-level region of evaporatively cooled downdraft air that spreads out horizontally beneath a precipitating convective system.

Owing to the importance of cold pools to heavy precipitation forecasts and the general lack of cold pool structures in model initial conditions, manual forecasting techniques are used to adjust operational model forecasts of rainfall totals in areas where cold pools are observed (Funk 1991). However, it also is important to find ways to improve the numerical forecasts of these situations by devising techniques that insert cold pools into model initial conditions (Stensrud and Fritsch 1994; Stensrud et al. 1999; Gallus and Segal 2001). Although these techniques clearly yield improvements in the depiction of mesoscale structures in the model initial conditions, improvements in the subsequent quantitative precipitation forecasts have been limited (Gallus and Segal 2001).

Another approach that may help capture realistic cold pool structures is a data assimilation system that uses situation-dependent covariances in the assimilation of surface data, such as the ensemble Kalman filter (Evensen 1994, 1997). This type of approach allows a single observation to modify the surrounding region in a manner that is dynamically and thermodynamically consistent with the local atmospheric flow characteristics. Using an ensemble Kalman filter assimilation approach, Hacker and Snyder (2005) show that surface observations alone are able to improve state estimates throughout the entire planetary boundary layer during both the daytime and nighttime. Thus, one or two observations from within a cold pool may be sufficient to generate a realistic three-dimensional cold pool structure in a model initial condition.

Analyses from an ensemble Kalman filter data assimilation system run routinely during the spring of 2007 are examined for cold pool structures. These analyses are designed to be used for mesoscale diagnostics and as initial conditions for a subsequent

model ensemble forecast. The assimilation system is described in section 2. Section 3 presents the results from two events, and a summary appears in section 4.

2. WRF ensemble Kalman filter data assimilation

The model chosen for use is the non-hydrostatic Advanced Research version of the Weather Research and Forecasting (WRF-ARW) model (Klemp 2004). The WRF model uses a terrain-following vertical coordinate and is designed for simulating both mesoscale and storm-scale phenomena as indicated by its ability to reproduce observed kinetic energy spectra (Skamarock 2004). The WRF model also includes a variety of options for physical process parameterization schemes. This model is quickly becoming the community model for mesoscale and storm-scale research and operational forecasting in the United States.

Surface data assimilation is conducted using the Data Assimilation Research Testbed (DART) developed at the National Center for Atmospheric Research (NCAR). The DART has been used for data assimilation studies with a variety of models, including WRF, and includes a parallel implementation that greatly increases its computational efficiency. Ensemble Kalman filters (Evensen 1996) update the probability distribution of an atmospheric state estimate, given an observation (and its associated error) and a prior estimate of the state's probability distribution, where the probability distribution is represented by the statistics of an ensemble. When the observation operators are approximately linear, ensemble data assimilation can be implemented in parallel on any number of computer processors as is done in the DART (Anderson and

Collins 2007). Further details of the ensemble-filtering algorithm used can be found in Anderson and Collins (2007).

For an ensemble size of 30 to 40, the ensemble Kalman filter has been shown to be very adept at generating realistic mesoscale structures in idealized (Zhang et al. 2006) and real data (Fujita et al. 2007) assimilation experiments. These results emphasize the unique capabilities of ensemble Kalman filters that can be applied to the mesoscale analysis problem. The ensemble Kalman filter approach is explicitly designed to produce an ensemble that is consistent with the error statistics of the analysis and very short-term forecasts. In addition, the filter approach incorporates flow-dependent covariance information. This leads to analysis increments that respect the structure of dynamically important features within the model, such as cold pools. The use of flow-dependent covariance information also ensures that relations between model variables are used advantageously to update unobserved variables. This last point is illustrated nicely by Snyder and Zhang (2003) who show how the covariance between radial velocity and vertical motion influences the analysis of vertical motion as a Doppler radar radial velocity observation is assimilated into a storm-scale simulation of a convective storm.

Hourly analyses are produced on a 30 km grid of 160x130 horizontal points and 30 vertical levels that covers the contiguous United States (Fig. 1). To start the data assimilation process, a forecast ensemble is needed. Thus, a 30-member WRF ensemble is created starting from initial and boundary conditions provided by the North American Model (NAM) of the National Centers for Environmental Prediction (NCEP) at 1200 UTC each day. Initial and boundary conditions are perturbed using the approach of Torn et al. (2006) based upon the covariance information provided by the WRF three-

dimensional variational analysis system. Soil moisture is perturbed using a Monte Carlo approach following Stensrud et al. (2000).

In addition to perturbing the initial and boundary conditions, the WRF model physical process schemes also are perturbed. Variations in land surface, planetary boundary layer, radiation, convection, and microphysical parameterizations are used to create a different set of model physics for each ensemble member as in Stensrud et al. (2000). Results from Fujita et al. (2007) indicate that an ensemble with combined physics and initial condition perturbations yields better analyses and forecasts than an ensemble system with only initial condition or physics perturbations. It appears that these two types of perturbations provide spread in different regions of the domain and via different processes, limiting the problems caused by large underdispersion seen in other ensemble systems.

A primary goal of this research is to evaluate the influence of surface observations on mesoscale analysis and numerical weather prediction. Therefore, after the initial ensemble is created at 1200 UTC from the NCEP NAM analysis (which itself incorporates numerous and various observations), only surface data are assimilated. Between 1500 and 1600 surface observations (Fig. 1) of 2-m potential temperature (θ), 2-m dewpoint temperature (T_d), and the 10-m horizontal winds (u, v) are assimilated every hour over an 18 h period from 1300 UTC the current day to 0600 UTC the following day using WRF-DART. Only observations from the standard surface sites maintained by national weather services are assimilated. A localization function for assimilating observations is used to reduce the impact of noisy background-error-covariance estimates associated with the finite ensemble size (Gaspari and Cohn 1999). A horizontal influence

radius of 300 km and a vertical influence radius of 20 model levels are selected following Fujita et al. (2007). The observational error standard deviations are assumed to be 2.0 K for θ and $T_{d,}$ and 2.0 m s^{-1} for u and $v,$ as determined by Zapotocny et al. (2000). The extrapolations from the model vertical levels to the 2-m and 10-m heights are calculated internally by the WRF and are consistent with the surface layer physical process parameterization schemes. Daily forecasts made from 15 March through 30 June 2007 are used to explore how well the ensemble Kalman filter produces cold pools when assimilating only surface data.

3. Results

National composite radar data from 15 March through 30 June 2007 are examined to identify mesoscale convective systems (MCSs), with convective lines of roughly 200 km in length or greater, that are not associated directly with frontal boundaries and occur between 1800 and 0600 UTC. This time window allows the ensemble Kalman filter to assimilate at least 6 h worth of surface observations prior to an examination of the output. A total of seven isolated MCSs are identified that fit the size criteria and time window, and also persist for several hours. In all of these cases, the ensemble mean analyses reproduce a cold pool associated with the MCS in roughly the correct location and time over several vertical model layers. Two cases are used to illustrate the types of features seen in the analyses.

3.1. 24-25 May 2007

Thunderstorms develop in the Oklahoma and Texas panhandles at 2100 UTC 23 May along a frontal boundary stretching from New Mexico to Kansas (not shown). The convection organizes into a line by 0500 UTC 24 May over the Texas panhandle and this convective line slowly increases in length as it moves to the southeast. The MCS is located in northern Texas 13 h later with a symmetric leading-line trailing-stratiform organization (Parker and Johnson 2000). The MCS begins propagating more to the south after 2200 UTC and dissipates near 0600 UTC 25 May. Very few reports of severe weather are associated with this convective system.

At 0200 UTC 25 May, the MCS has an arc-shaped leading-line trailing-stratiform organization and is centered over Texas (Fig. 2). Numerous convective cells have reflectivities greater than 55 dBZ, although the leading convective line is discontinuous. A large stratiform precipitation region extends northward from the convective line for over 150 km. Surface observations show a convergence zone is associated with the arc-shaped convective line with southeasterly winds to the south and northwesterly to northeasterly winds to the north (Fig. 3). Near the northern end of the stratiform rain region, the surface winds shift to southeasterly again producing a divergent zone at the surface. Surface temperatures to the south of the MCS are near 298 K, whereas temperatures within the cold pool in the convective region are colder and vary between 295 and 291 K.

The ensemble mean analysis of 2-m temperature and lowest model level winds, produced after 14 h of surface data assimilation, shows structures that closely resemble

the observations (Fig. 4). There is a strong baroclinic zone running parallel to the observed arc-shaped convective line, with temperatures above 296 K to the south and below 294 K to the north. The flow is convergent along this baroclinic zone and divergent to the north underneath the stratiform precipitation region (Fig. 2). While the surface observations suggest the observed temperature gradient may have been slightly stronger, the ensemble mean analysis appears to be a very reasonable representation of the situation at this time. Root mean square differences across the entire model domain between observations and the ensemble mean are near 1.6 K for most analysis times (not shown), with the analyses being too cool during the daytime and too warm at night by approximately 0.5 K. Thus, the analyses have a slightly reduced diurnal cycle.

The vertical extent of the analyzed cold pool is seen in horizontal temperature plots for higher model layers (not shown) and in the vertical velocity fields. The ensemble mean vertical velocities for the fifth model layer at approximately 500 m above ground level (Fig. 5) indicate that the region of upward vertical motion largely overlies the arc-shaped convective line (Fig. 2). In addition, the regions of enhanced upward motion largely correspond with the regions of higher radar reflectivities seen in northeastern Texas and central Texas along the convective line. Sinking motion is found within the stratiform precipitation region and above the area of surface divergence (Fig. 4). A narrow zone of upward motion is found at the northern edge of the trailing stratiform rain region and above a zone of surface convergence.

The influence of the surface observations on the ensemble analysis is investigated by calculating the difference in the ensemble mean before and after all surface observations are assimilated at a specific time. Results from assimilating surface

observations at 0200 UTC 25 May show that the surface observations cooled the atmosphere in the lowest 1 km above ground level in the region of the mesoscale convective system (Fig. 6). Cooling near the ground surface is strongest near the leading convective line where the observations also produce stronger northwesterly winds (Fig. 6a). Above the surface, the assimilation of surface observations yields regions of both cooling and warming, with the cooling again located near the leading convective line (Fig. 6b). The region of warming is restricted to the northern edge of the trailing stratiform precipitation region. The assimilation also tends to dry the environment underneath the mesoscale convective system (not shown). Smaller differences are found in the environment surrounding the convective system, indicating that the initial analysis of the atmospheric state is in reasonable agreement with the surface observations.

Soundings from within the cold pool at Llano, Texas, and from ahead of the MCS at Victoria, Texas, also highlight the ability of the ensemble Kalman filter assimilation technique to reproduce a realistic cold pool structure. The soundings from within the cold pool show a nearly isothermal low-level temperature structure up to 900 hPa and lapse rates approaching moist adiabatic above this level (Fig. 7). Compared to the soundings ahead of the MCS (Fig. 8), the atmosphere has higher relative humidities in and above the cold pool (Fig. 7). This is especially true for the surface to 700 hPa and 400 to 200 hPa layers. Thus, not only are the surface data influencing the low-levels of the model, but through interaction with the convective parameterization schemes are also influencing the atmosphere throughout the troposphere.

3.2. 19-20 June 2007

Thunderstorms develop ahead of a frontal boundary around 2200 UTC 19 June in the Texas panhandle and northcentral Oklahoma. By 0200 20 June two arc-shaped intense convective lines have propagated to the south and grown upscale. These two lines merge over southwestern Oklahoma at 0530 UTC and have a well-defined leading-line trailing-stratiform organization (Fig. 9). This single MCS moves south and dissipates over southern Texas at 1700 UTC. Numerous reports of damaging winds are associated with this derecho-producing convective system (Johns and Hirt 1987), with the earlier storms also producing hail.

The 2-m observations show temperatures above 299 K to the south of the MCS and between 289 and 295 K underneath the MCS (Fig. 10). Winds at 10 m are generally southeasterly ahead of the MCS and are stronger and have a northerly component behind the convective line. There is a large divergent region that stretches from westcentral Oklahoma into the Texas panhandle underneath the trailing stratiform precipitation region. The ensemble mean analysis captures very similar structures, including the strong temperature gradient along the cold pool leading edge, the southeasterly winds ahead of the cold pool and the northerly component to the winds behind the cold pool, and the divergent flow over northcentral Oklahoma (Fig. 11). Through the assimilation process, strong temperature gradients are maintained in southwest Oklahoma and northwest Texas (Fig. 11) despite the sparse observations in this region (Fig. 10). Plots of ensemble mean altimeter setting indicate an increase in pressure of 6 hPa associated with the passage of the cold pool (Fig. 12), in agreement with the observed (not shown)

surface pressure rise in southwestern Oklahoma at Altus and slightly less than the 9 hPa pressure increase at Childress, Texas near the region where the two lines merge.

The ensemble mean analysis of vertical velocity at approximately 1 km above ground level shows a distinct arc-shaped region of upward motion (Fig. 13) over the location of the observed convective line (Fig. 9). Vertical velocities in excess of 0.8 m s^{-1} are seen where the two convective lines meet, with subsidence again indicated in the trailing stratiform region. Thus, through the assimilation of only surface data (and through the model responses to the assimilated observations), the ensemble analyses are producing realistic vertical motion fields well above the surface. Particularly noteworthy is the zone of northerly flow towards the convective line (rear inflow) to the north of the region where the two convective lines meet (Fig. 13). This flow pattern is not seen in the surface observations, yet rear inflow is commonly observed in mesoscale convective systems (Smull and Houze 1987). Radial wind observations from a Doppler radar at Frederick, Oklahoma, show rear inflow at approximately 2 km above ground level (not shown) in the same region where rear inflow is produced in the ensemble analysis. Furthermore, the middle portion of the combined convective line is observed to propagate southward the fastest over the next 2 h, a behavior that is consistent with the effects of a rear inflow jet in a derecho-producing convective system (Weisman 1993).

The influence of the surface observations on the ensemble analysis for this case is investigated by calculating the difference in the ensemble mean before and after all surface observations are assimilated at a specific time. Results from assimilating surface observations at 0600 UTC 20 June show that the surface observations cooled the atmosphere in the lowest 1 km above ground level in the region of the mesoscale

convective system (Fig. 14). Cooling near the ground surface is strongest near the leading convective line where the observations also produce stronger northwesterly winds (Fig. 14a). Above the surface, the assimilation of surface observations yields a broader region of cooling, with the maximum cooling again located near the leading convective line (Fig. 14b). Note the increased northerly winds near the region where the convective lines meet that are produced by the surface data assimilation and lead to the region of rear inflow. The assimilation also tends to dry the environment underneath the mesoscale convective system (not shown). As seen in the May case, smaller differences are found in the environment surrounding the convective system, indicating that the initial analysis of the atmospheric state is in reasonable agreement with the surface observations.

Ensemble analysis soundings from Gage, Oklahoma, near the northern edge of the stratiform rain region show an isothermal layer from the surface to near 850 hPa that is associated with the cold pool (Fig. 15). The surface observations are clearly influencing the atmospheric structure in at least the lowest km and perhaps even higher. In addition, a number of the individual moisture profiles from the ensemble members suggest an onion-like structure that is typical of the trailing regions of MCSs (Zipser 1977) and often associated with mesolows (Johnson et al. 1989). The ensemble mean surface altimeter field suggests a weak mesolow is located just to the north of Gage (Fig. 12). This result suggests that the assimilation of surface observations alone are able to produce realistic horizontal fields of temperature, moisture, and winds, along with vertical structures that are known to be associated with these surface features.

4. Summary

Results from analyses created through the ensemble Kalman filter assimilation of surface data into a mesoscale WRF ensemble show that the analyses create realistic structures in association with MCSs during the two days examined. In particular, the analyses capture the cold pools that occur underneath MCSs and play an important role in their evolution. Not only is the ensemble Kalman filter able to produce realistic surface analyses that compare well with the available observations, but it also produces vertical motions and vertical structures within and above the boundary layer that are known to be associated with these observed surface features. In particular, a rear inflow jet behind the main convective line is created along with an onion sounding along the back edge of the trailing stratiform precipitation region. Both of these structures are known to be associated with MCSs, and rear inflow is observed in the area indicated by the ensemble analysis by the Frederick, Oklahoma, radar. The ability of the ensemble Kalman filter assimilation to produce such important mesoscale structures is encouraging.

While the assimilation of only surface observations is shown to be very beneficial to the creation of realistic mesoscale features associated with MCSs, other routine observations provide more opportunities for producing high-quality analyses that can be used to start ensemble model forecasts. Observations from rawinsondes, wind profilers, and radio occultation data can also assist in producing the mesoscale structures needed to correctly predict convective development and evolution. Future work will seek to ingest these other data sets along with surface pressure observations into the ensemble Kalman filter system and evaluate the resulting ensemble analyses and forecasts that start from

these analyses.

Acknowledgments

The authors would like to thank Nancy Collins, Jeff Anderson, and Chris Snyder for their assistance with the data-assimilation system; Jack Kain, Steve Weiss, David Bright, and all the participants during the 2007 Spring Forecasting Experiment for their help in evaluating the mesoscale analyses; and Mary Haley and Lou Wicker for their assistance with NCL graphics. Composite radar images were obtained from http://www.mmm.ucar.edu/imagearchive/. Partial funding was provided by NOAA/Office of Oceanic and Atmospheric Research under NOAA-University of Oklahoma Cooperative Agreement #NA17RJ1227, U.S. Department of Commerce.

References

Anderson, J. L., and N. Collins, 2007: Scalable implementations of ensemble filter algorithms for data assimilation. *J. Atmos. Oceanic Technol*., **8,** 1452-1463.

Atkinson, B. W., 1981: *Meso-scale atmospheric circulations*. Academic Press, 495 pp.

Evensen, G., 1994: Sequential data assimilation with a nonlinear quasigeostrophic model using Monte Carlo methods to forecast error statistics. *J. Geophys. Res*., **99**(C5), 10143-10162.

_____, 1997: Advanced data assimilation for strongly nonlinear dynamics. *Mon. Wea. Rev.,* **125,** 134201354.

Fujita, T., Stensrud D. J., Dowell D. C., 2007: Surface data assimilation using an ensemble Kalman filter approach with initial condition and model physics uncertainty. *Mon. Wea. Rev.,* **135,** 1846-1868.

Fujita, T., 1963: Analytical mesometeorology: A review. *Meteor. Monographs,* Amer. Meteor. Soc., **5**, 77-125.

Funk, T. W., 1991: Forecast techniques utilized by the Forecast Branch of the National Meteorological Center during a major convective rainfall event. *Wea. Forecasting,* **6**, 548-564.

Gallus, W. A., Jr., and M. Segal, 2001: Impact of improved initialization of mesoscale features on convective system rainfall in 10-km Eta simulations. *Wea. Forecasting,* **16**, 680-696.

Gaspari, G., and S. E. Cohn, 1999: Construction of correlation functions in two and three dimensions. *Quart. J. Roy. Meteor. Soc.,* **125,** 723-757.

Hacker, J. P., and C. Snyder, 2005: Ensemble Kalman filter assimilation of fixed screen-height observations in a parameterized PBL. *Mon. Wea. Rev*., **133**, 3260-3275.

Johns, R. H., and C. A. Doswell III, 1992: Severe local storms forecasting. *Wea. Forecasting,* **7**, 588-612.

_____, and W. D. Hirt, 1987: Derechos: Widespread convectively induced windstorms. *Wea. Forecasting,* **2**, 32-49.

Johnson, R. H., S. Chen, and J. J. Toth, 1989: Circulations associated with a mature-to-decaying midlatitude mesoscale convective system. Part I: Surface features - heat bursts and mesolow development. *Mon. Wea. Rev*., **117**, 942-959.

Klemp, J., 2004: Next-generation mesoscale modeling: A technical overview of WRF. *Preprints*, 20th Conf. Wea. Analysis and Forecasting, Seattle, WA, Amer. Meteor. Soc., Paper 11.2.

Olson, D. A., 1985: The impact of existing boundaries on the usefulness of operational model QPF. Preprints, Sixth Conf. on Hydrometeorology, Indianapolis, IN, Amer. Meteor. Soc., 277-283.

Parker, M. D., and R. H. Johnson, 2000: Organizational modes of midlatitude mesoscale convective systems. *Mon. Wea. Rev.,* **128**, 3413-3436.

Schaefer, J. T., 1974: The life cycle of the dryline. *J. Appl. Meteor.,* **13**, 444-449.

Smull, B.F., and R.A. Houze, 1987: Dual-Doppler radar analysis of a midlatitude squall line with a trailing region of stratiform rain. *J. Atmos. Sci.*, **44**, 2128–2149.

Snyder, C., and F. Zhang, 2003: Assimilation of simulated Doppler radar observations with an ensemble Kalman filter. *Mon. Wea. Rev.,* **131**, 1663-1677.

Skamarock, W. C., 2004: Evaluating NWP models using kinetic energy spectra. *Mon. Wea. Rev.,* **132,** 3019-3032.

Stensrud, D.J., and J.M. Fritsch, 1994: Mesoscale convective systems in weakly forced large-scale environments. Part III: Numerical simulations and implications for operational forecasting. *Mon. Wea. Rev.*, **122**, 2084-2104.

_____, G. Manikin, E. Rogers, and K. Mitchell, 1999: Importance of cold pools to mesoscale model forecasts. *Wea. Forecasting*, **14**, 650-670.

_____, N. Yussouf, M. E. Baldwin, J. T. McQueen, J. Du, B. Zhou, B. Ferrier, G. Manikin, F. M. Ralph, J. M. Wilczak, A. B. White, I. Djlalova, J.-W. Bao, R. J. Zamora, S. B. Benjamin, P. A. Miller, T. L. Smith, T. Smirnova, and M. F. Barth, 2006: The New England High-Resolution Temperature Program (NEHRTP). *Bull. Amer. Meteor. Soc.,* **87,** 491-498.

Torn, R. D., Hakim G. J., Snyder C., 2006: Boundary conditions for limited-area ensemble Kalman filters. *Mon. Wea. Rev.,* **134,** 2490-2502.

Weisman, M.L., 1993: The genesis of severe, long-lived bow echoes. *J. Atmos. Sci.*, **50**, 645–670.

Zhang, F., Z. Meng, and A. Aksoy, 2006: Tests of an ensemble Kalman filter for mesoscale and regional-scale data assimilation. Part I: Perfect model experiments. *Mon. Wea. Rev.,* **134,** 722-736.

Zipser, E. J., 1977: Mesoscale and convective-scale downdrafts as distinct components of squall-line circulation. *Mon. Wea. Rev.,* **105,** 1568-1589.

Figure captions

Figure 1. Model domain used in this study. Gray circles indicate surface observation sites used in the data assimilation. The actual distribution of surface observations varies from hour to hour depending upon data availability.

Figure 2. Composite reflectivity data (dBZ) over Texas on 0200 UTC 25 May 2007 at 2 km resolution. Values above 5 dBZ are shaded and change shade every 5 dBZ. Values above 40 dBZ are black, while values above 50 dBZ are a lighter gray surrounded by black as seen along the southern edge of the convective region. States of Texas (TX) and Oklahoma (OK) indicated. Courtesy of the image archive at NCAR.

Figure 3. Surface observations of 2-m temperature (K), altimeter pressure (hPa), and 10-m winds (full barb 10 m s^{-1}) over Texas (TX) and Oklahoma (OK) valid at 0200 UTC 25 May 2007. Also shown is the outline of the convective line depicted in Fig. 2 (gray) and a station model in the lower right where TTT is temperature and PP is altimeter pressure - 1000 hPa.

Figure 4. Ensemble mean analysis of 2-m temperature (K) and lowest model level winds (maximum vector length is 11.4 m s^{-1}) valid at 0200 UTC 25 May 2007. Also shown is the general outline of the convective line depicted in Fig. 2 (black line). The location of the sounding in Fig. 7 indicated by a circle.

Figure 5. Ensemble mean analysis of vertical velocity (m s^{-1}) and horizontal winds (maximum vector length is 18.5 m s^{-1}) for model level 5, located at roughly 500 m above ground level, valid at 0200 UTC 25 May 2007. Regions of upward motion

are connected by the gray lines. Also shown is the general outline of the convective line depicted in Fig. 2 (black line).

Figure 6. Difference in ensemble mean temperature (K) and winds (vectors) before and after all surface observations are assimilated at 0200 UTC 25 May 2007 for (a) the lowest model level and (b) the 7th model level at approximately 750 m above ground level. Regions of warming are connected by the gray line in (b). Wind vector magnitudes shown in each panel. The general outline of the convective line as depicted in Fig. 2 is shown by a black line.

Figure 7. Skew-T log p plot of the temperature (black) and water vapor (gray) profiles from the grid point closest to Llano, Texas (AQO), located within the cold pool of the MCS, valid at 0200 UTC 25 May 2007. Thick lines show the ensemble mean, while thin lines show the soundings from each of the 30 ensemble members. Location of AQO shown in Fig. 4.

Figure 8. As in Figure 7, but from the grid point closest to Victoria, Texas (VCT), approximately 300 km southeast of AQO and located to the south of the MCS.

Figure 9. Composite reflectivity data (dBZ) over Oklahoma (OK) and Texas (TX) on 0600 UTC 20 June 2007 at 2 km resolution. Values above 5 dBZ are shaded and change shade every 5 dBZ. Values above 40 dBZ are black, while values above 50 dBZ are a lighter gray surrounded by black as seen along the southern edge of the convective region. Courtesy of the image archive at NCAR.

Figure 10. Surface observations of 2-m temperature (K), altimeter pressure (hPa), and 10-m winds (full barb 10 m s^{-1}) over Oklahoma (OK) and Texas (TX) valid at 0600 UTC 20 June 2007. Also shown is the outline of the convective line

depicted in Fig. 9 (gray) and a station model in the lower right where TTT is temperature and PP is altimeter pressure - 1000 hPa.

Figure 11. Ensemble mean analysis of 2-m temperature (K) and lowest model level winds (maximum vector length is 15.9 m s^{-1}) valid at 0600 UTC 20 June 2007. Also shown is the general outline of the convective line depicted in Fig. 9 (black line). The location of the sounding in Fig. 15 indicated by a circle.

Figure 12. Ensemble mean analysis of altimeter setting (hPa) and lowest model level winds (maximum vector length is 15.9 m s^{-1}) valid at 0600 UTC 20 June 2007. Also shown is the general outline of the convective line depicted in Fig. 9 (black line).

Figure 13. Ensemble mean analysis of vertical velocity (m s^{-1}) and horizontal winds (maximum vector length is 14.9 m s^{-1}) for model level 9, located at roughly 1 km above ground level, valid at 0600 UTC 20 June 2007. Regions of upward motion are connected by the gray line. Also shown is the general outline of the convective line depicted in Fig. 9 (black line).

Figure 14. Difference in ensemble mean temperature (K) and winds (vectors) before and after all surface observations are assimilated at 0600 UTC 20 June 2007 for (a) the lowest model level and (b) the 9th model level at approximately 1 km above ground level. Cooling is occurring within the region of the mesoscale convective system at both levels. Wind vector magnitudes shown in each panel. The general outline of the convective line as depicted in Fig. 9 is shown by a black line.

Figure 15. Skew-*T* log *p* plot of the temperature (black) and water vapor (gray) profiles from Gage, Oklahoma (GAG), located within the cold pool of the MCS, valid at

0600 UTC 20 June 2007 (location shown in Fig. 11). Thick lines show the ensemble mean, while thin lines show the soundings from each of the 30 ensemble members.

Figure 1

Click here to download high resolution image

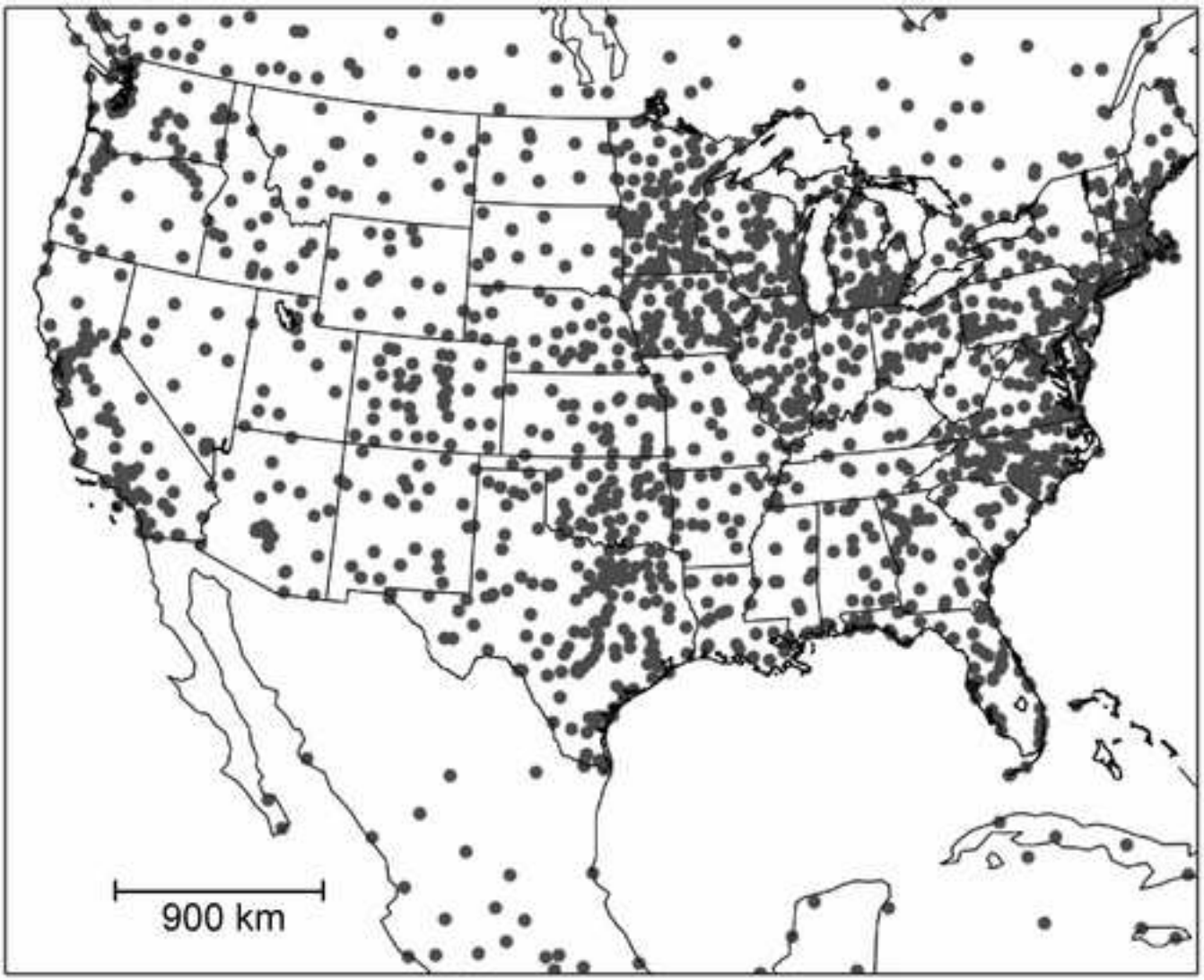

Figure 2

Click here to download high resolution image

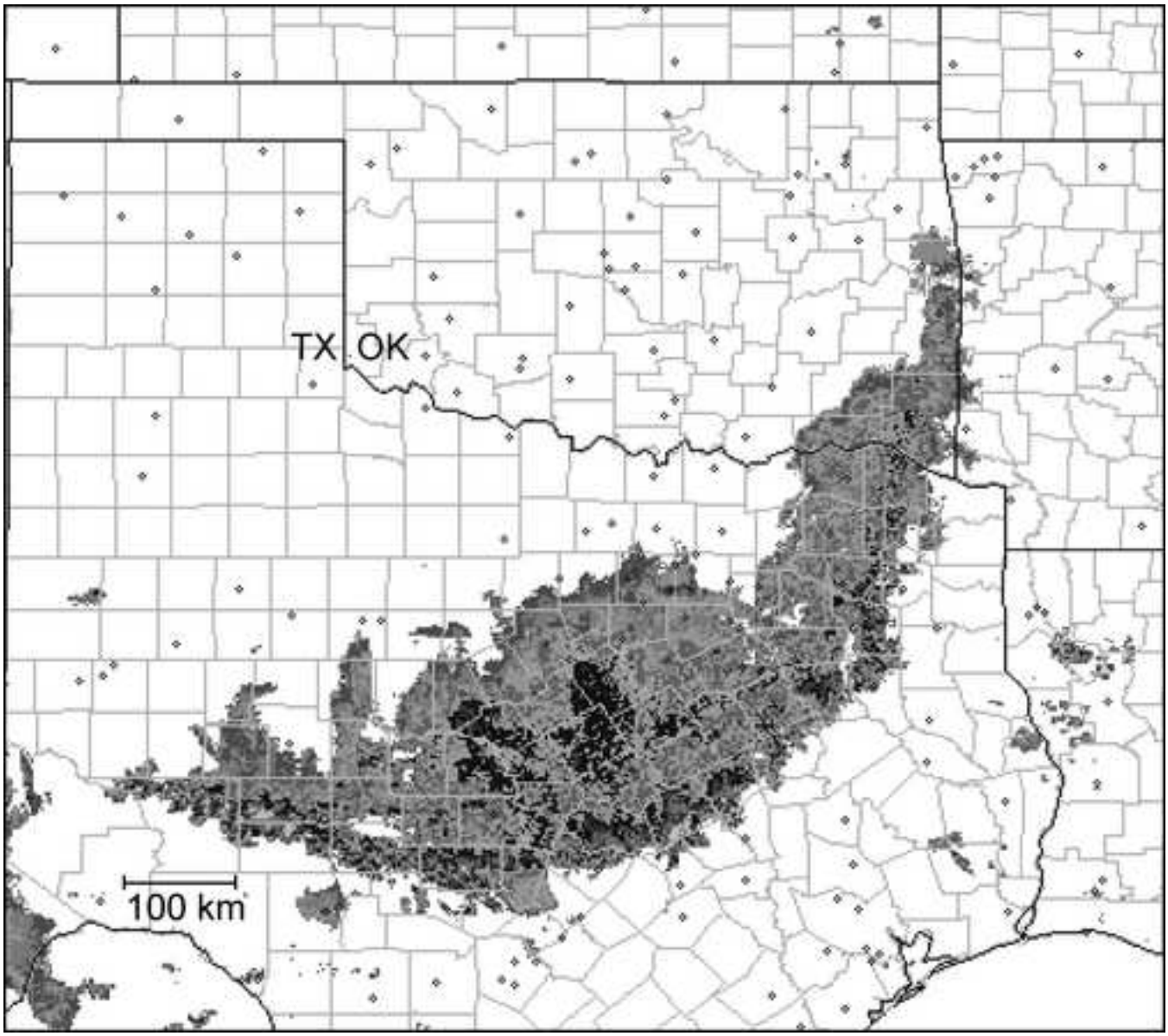

Figure 3

Click here to download high resolution image

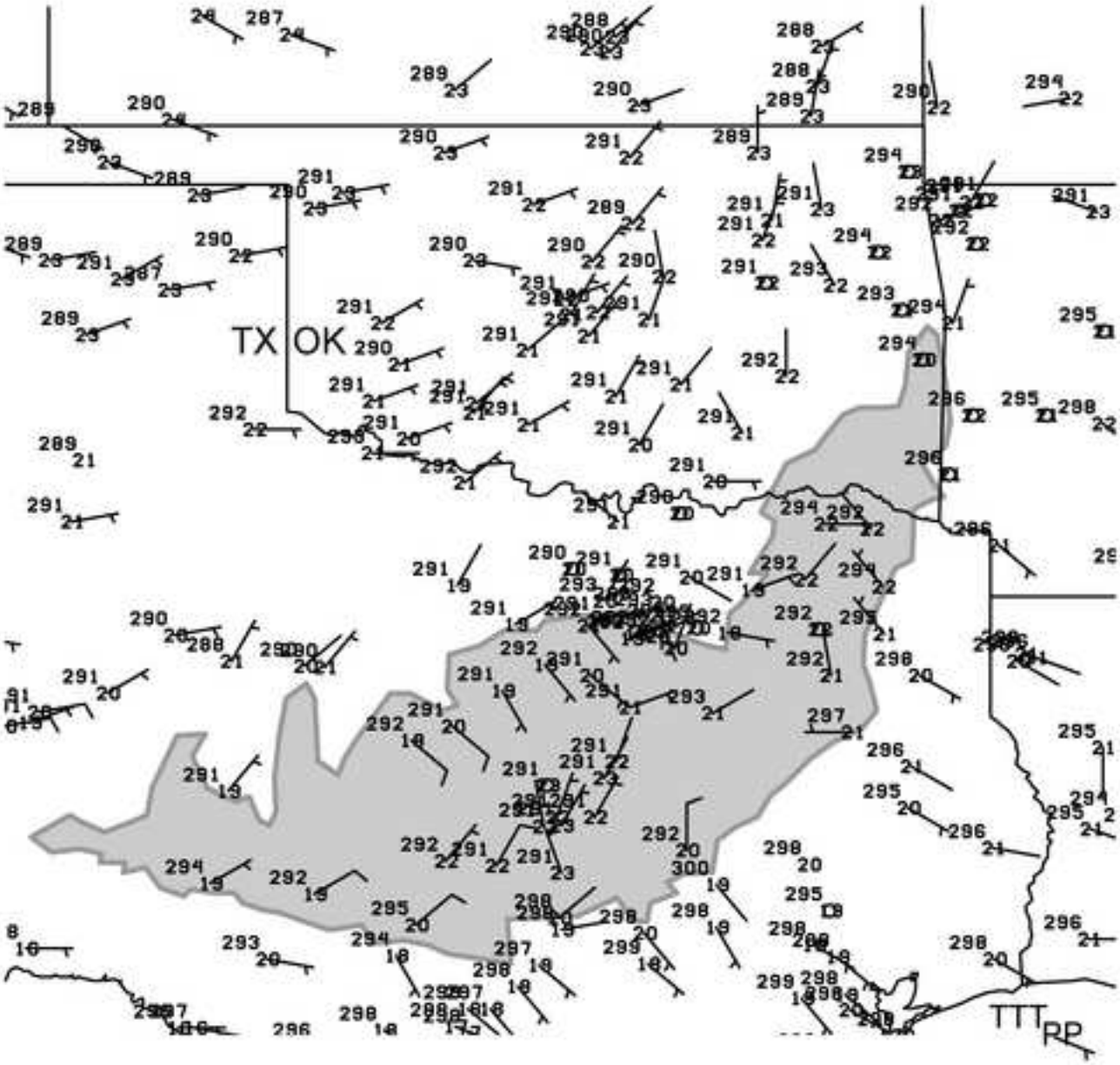

Figure 4

Click here to download high resolution image

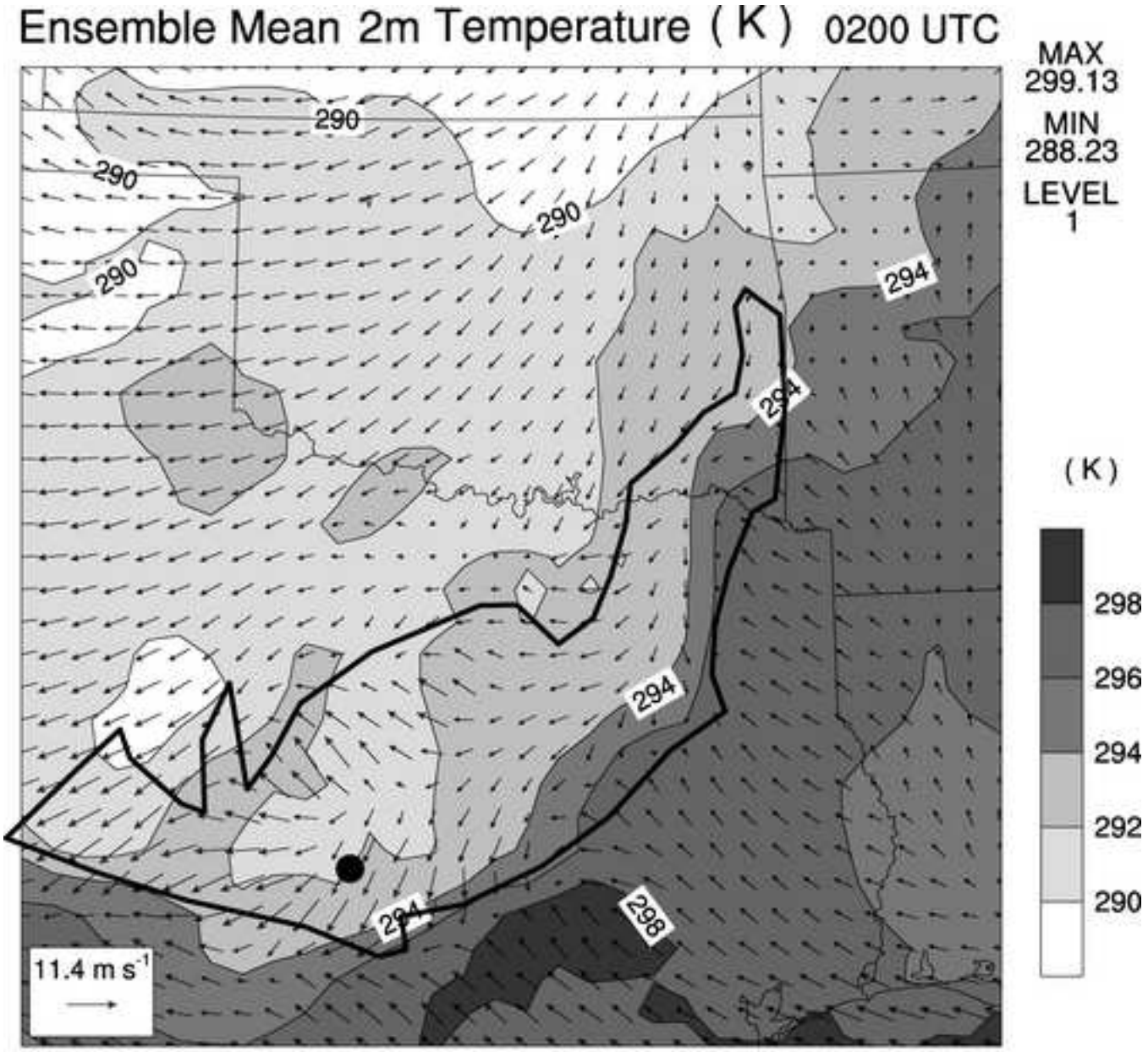

Figure 5

Click here to download high resolution image

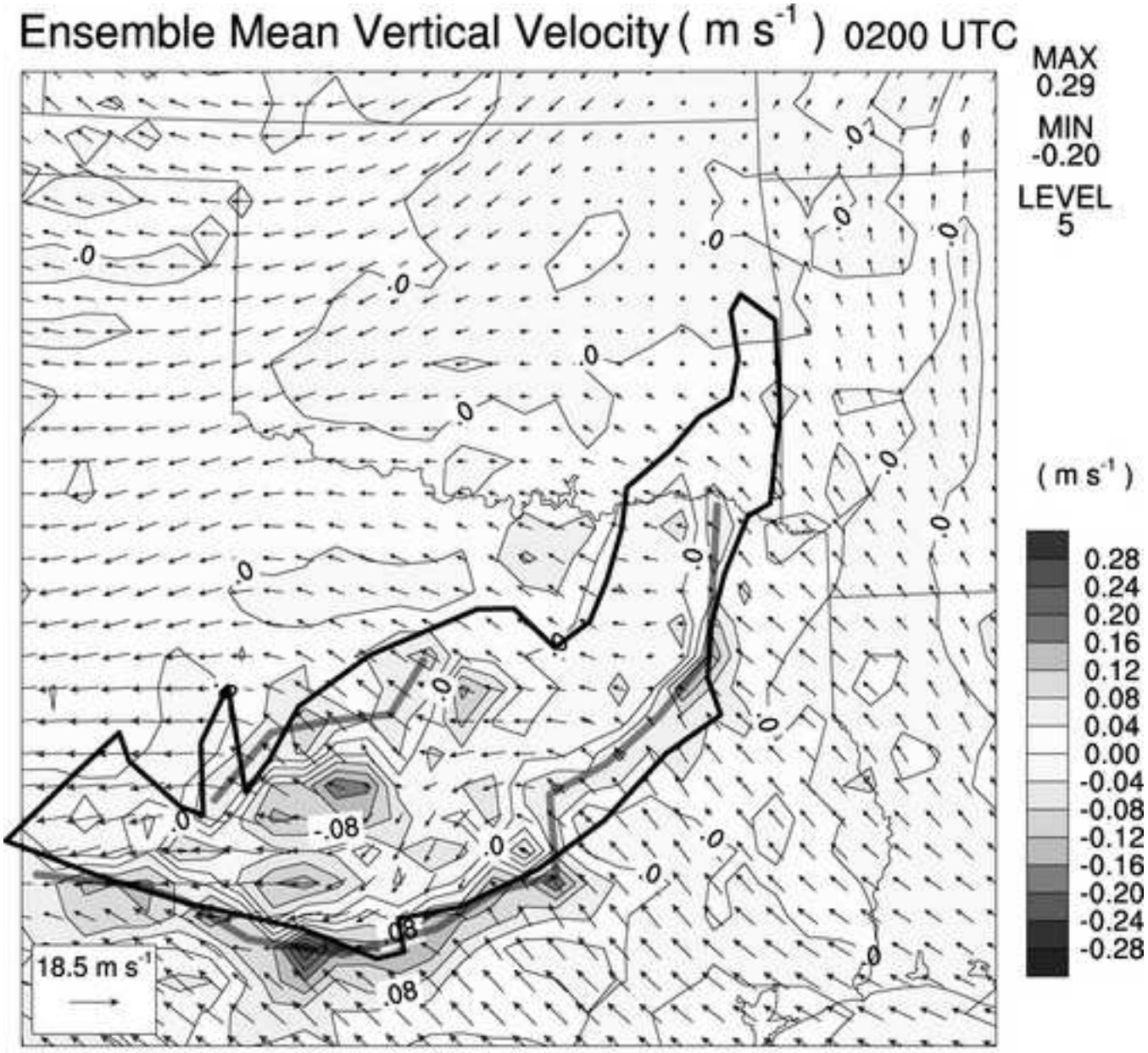

Figure 6

Click here to download high resolution image

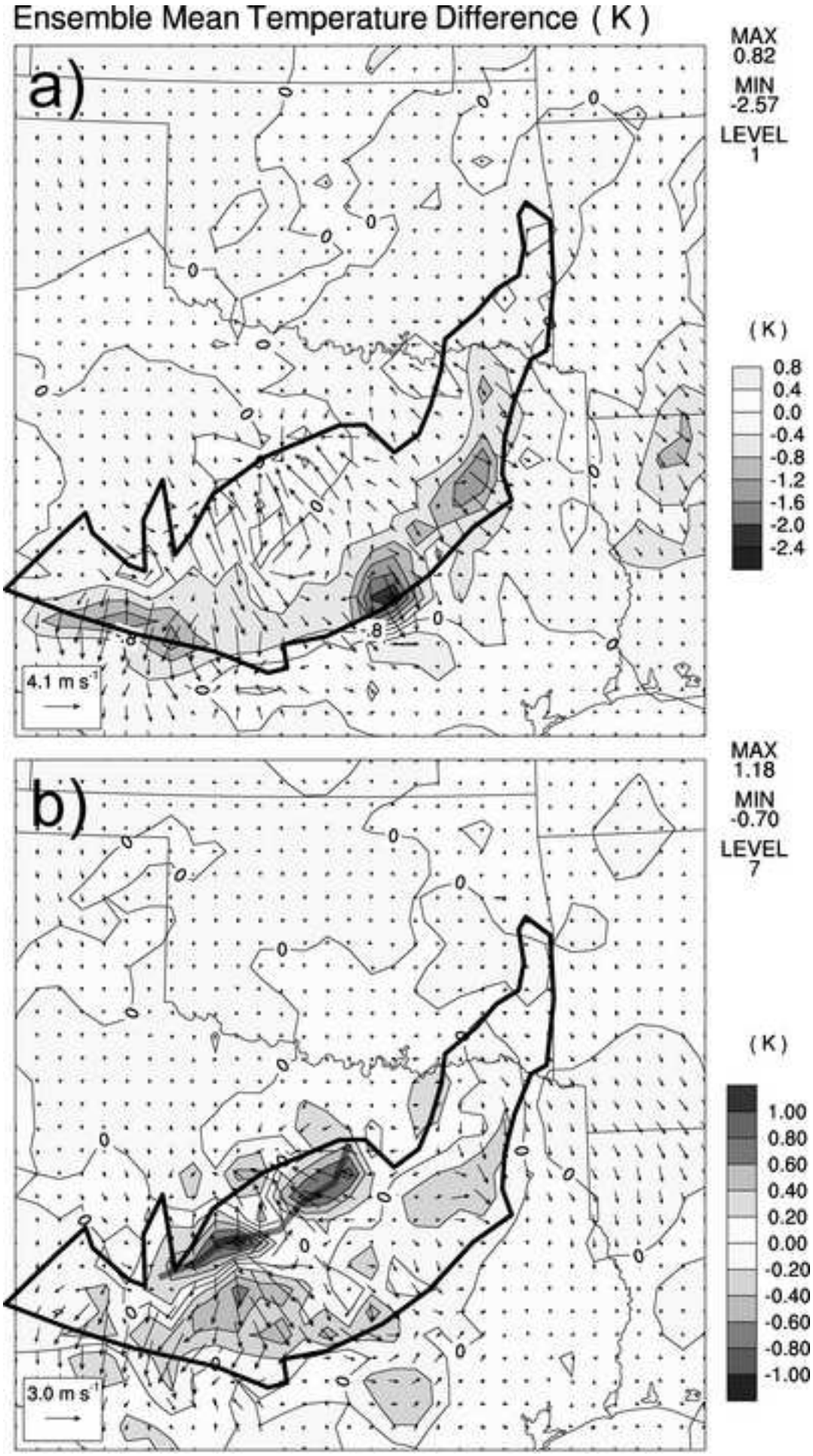

Figure 7

Click here to download high resolution image

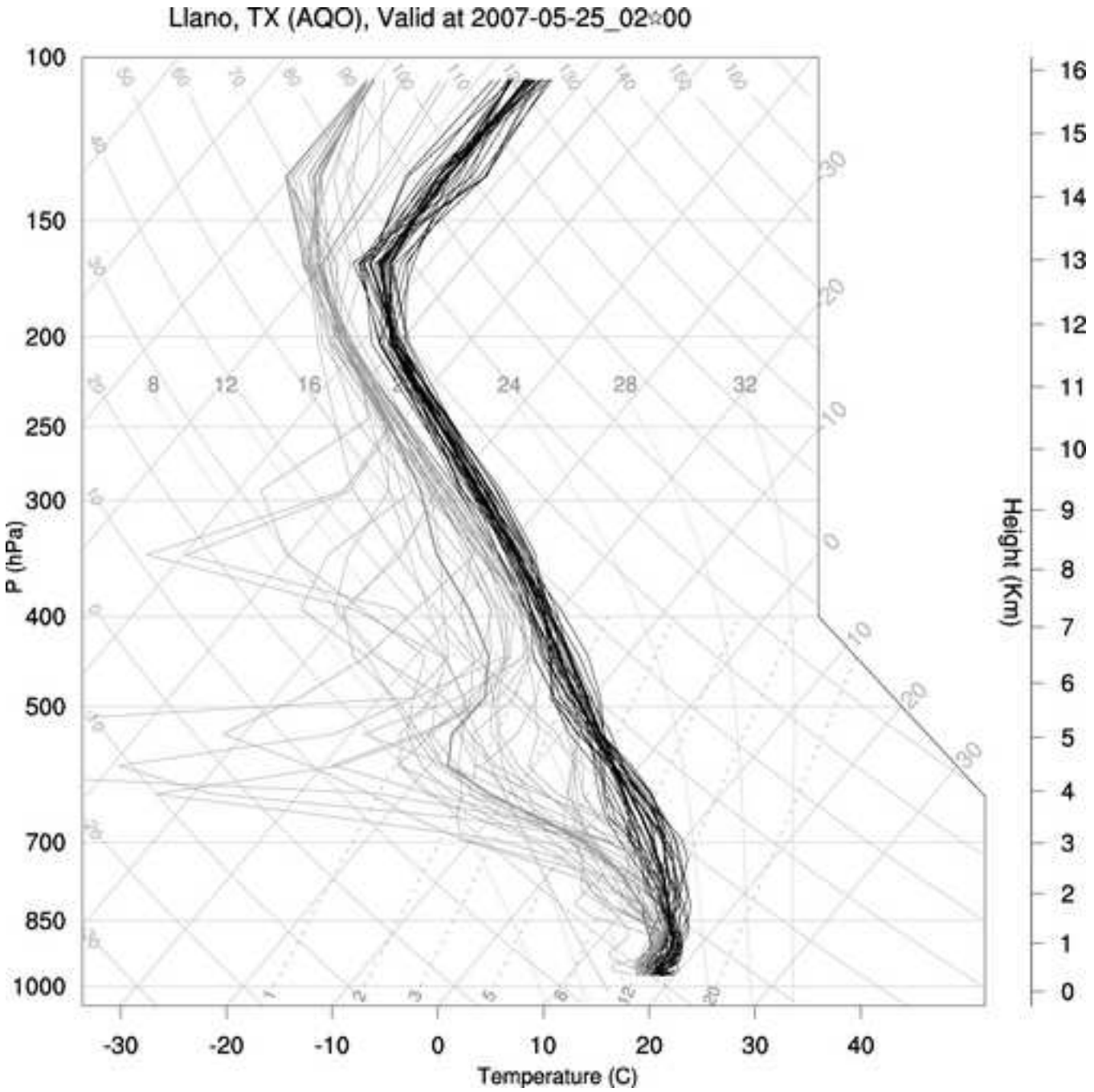

Figure 8

Click here to download high resolution image

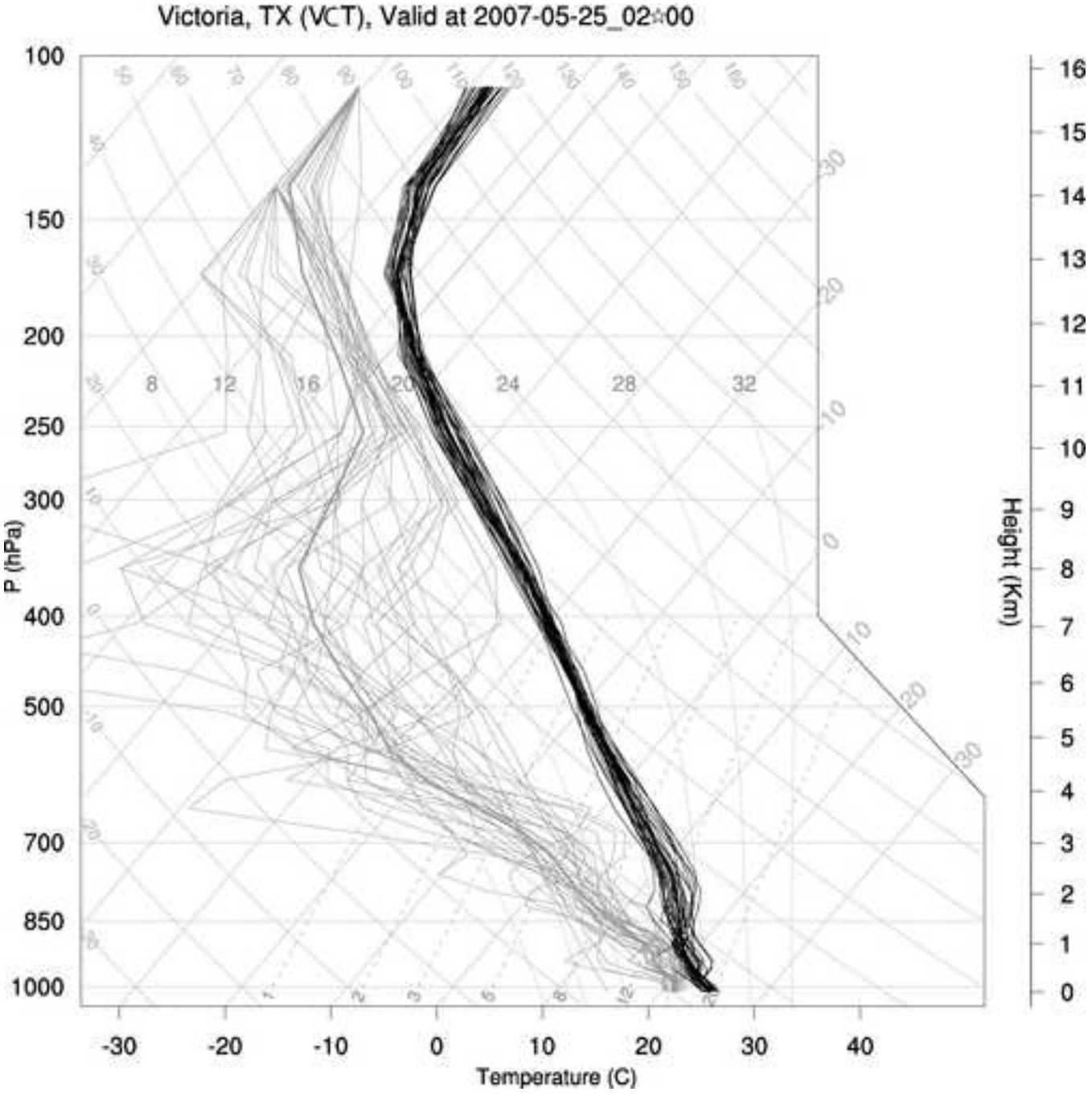

Figure 9

Click here to download high resolution image

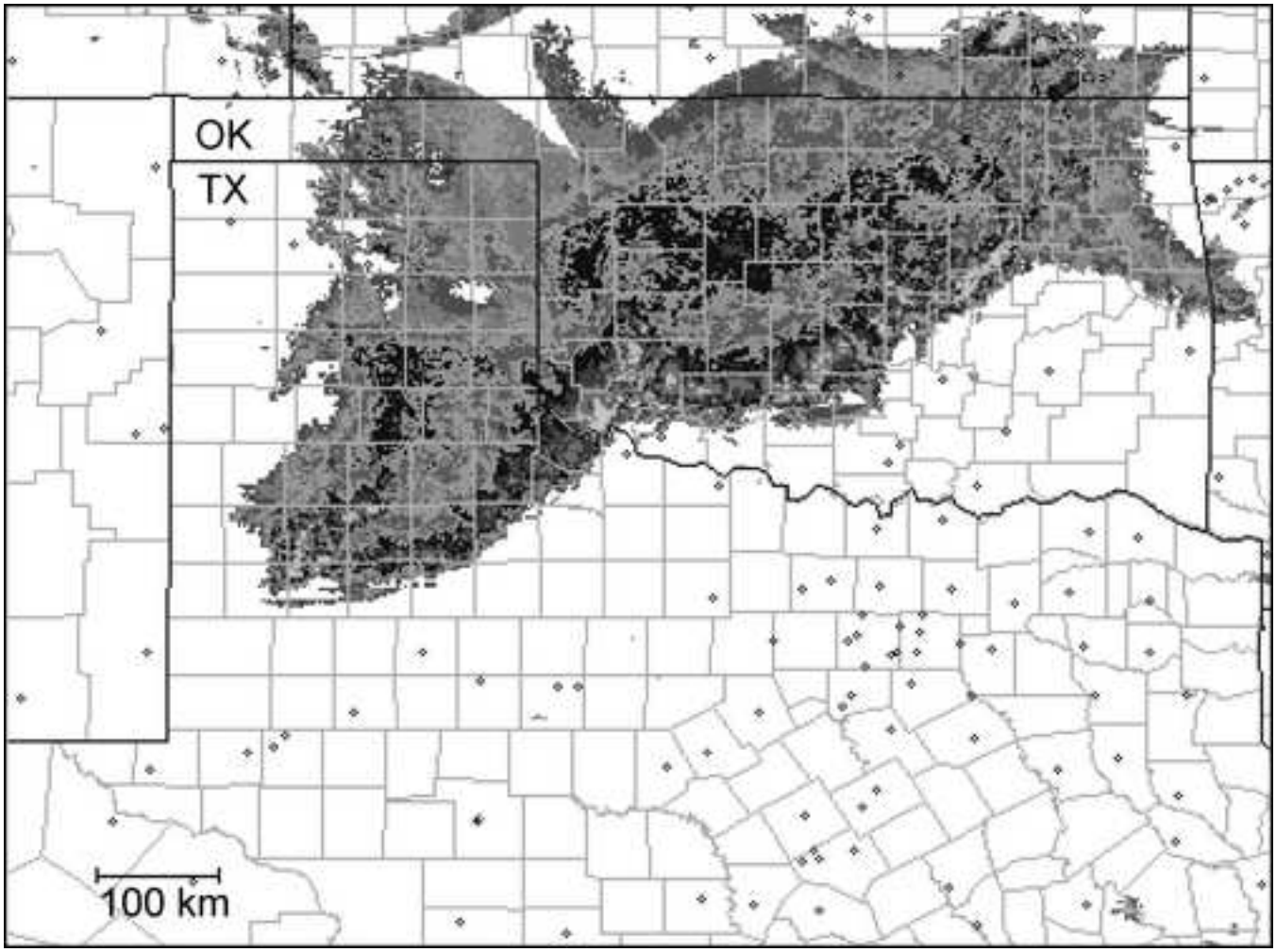

Figure 10

Click here to download high resolution image

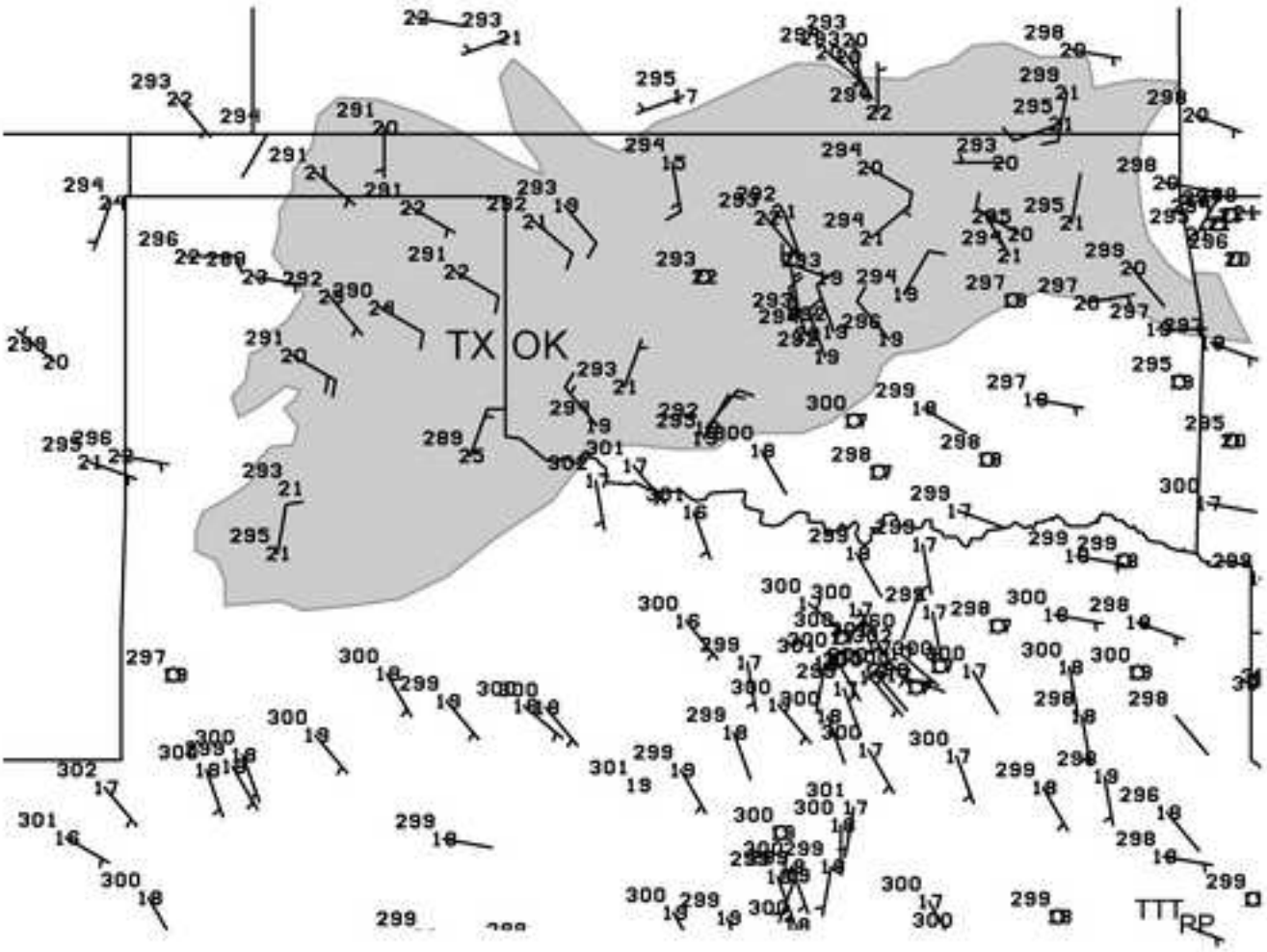

Figure 11

Click here to download high resolution image

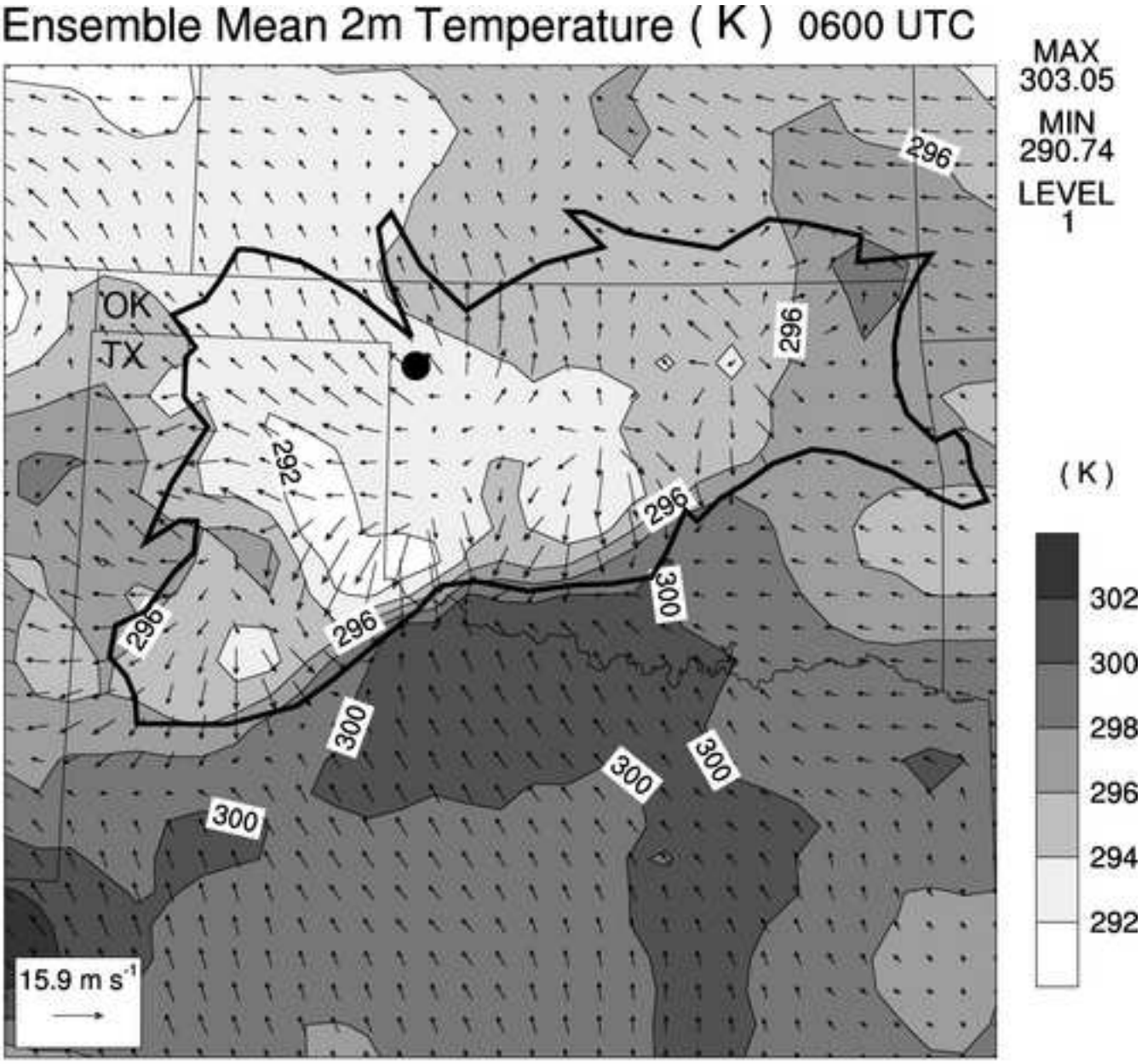

Figure 12

Click here to download high resolution image

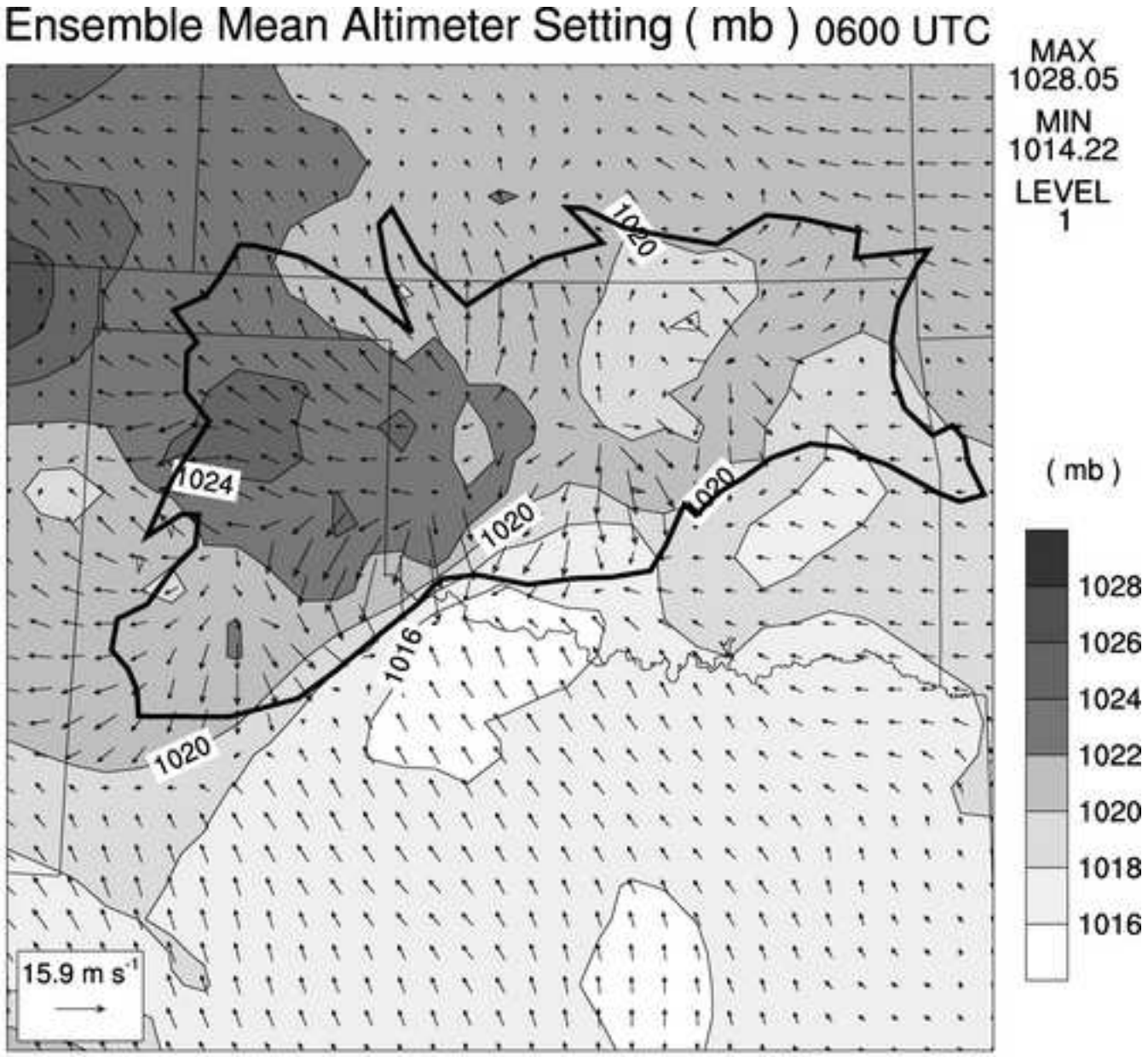

Figure 13

Click here to download high resolution image

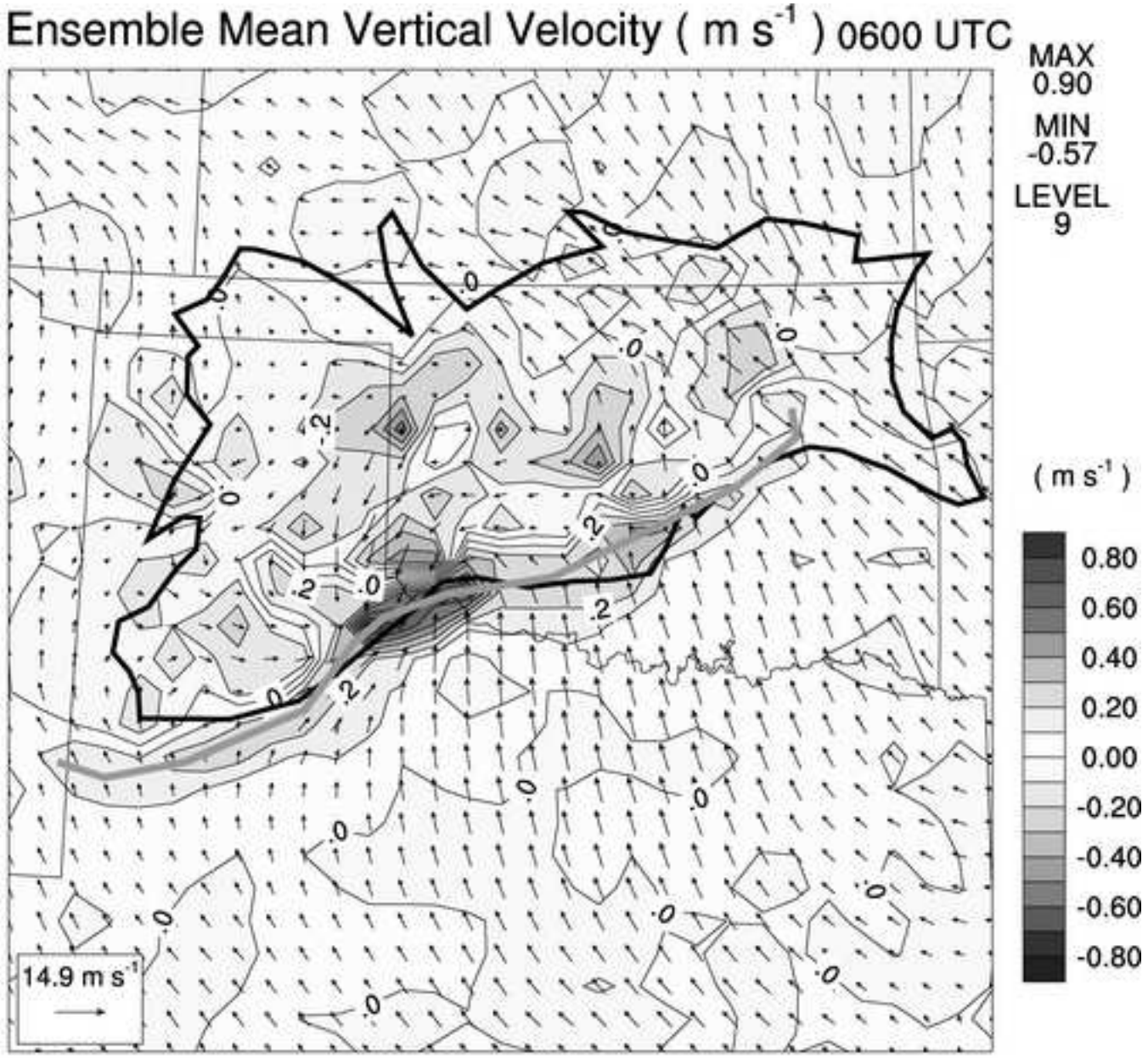

Figure 14

Click here to download high resolution image

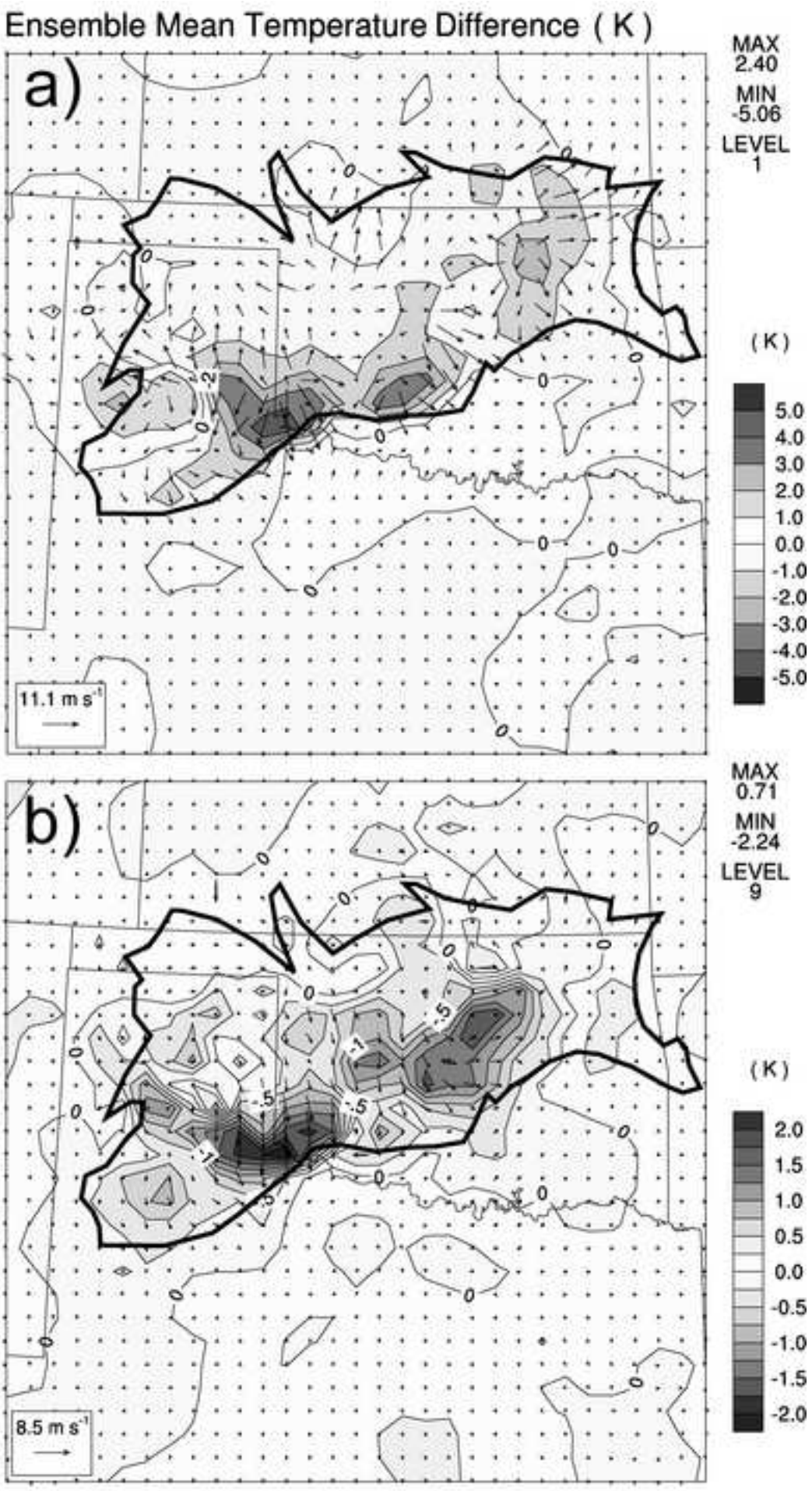

Figure 15

Click here to download high resolution image